Phase diagrams of charged colloidal particles

Wan Y. Shih, Ilhan A. Aksay, and Ryoichi Kikuchi
Department of Materials Science and Engineering, University of Washington, Seattle, Washington 98195

(Received 22 December 1986; accepted 26 January 1987)

We have calculated the phase diagrams of charged colloidal particles in the parameter space. The free energies of different phases, which were used to determine the phase boundaries, were calculated variationally. The Einstein oscillators and the hard sphere fluid were used as the reference systems for the solid phases and the liquid, respectively. The interparticle interactions were approximated to be the Debye–Hückel screened Coulomb potential with size correction. We show that the solid phases are stable at low salt concentrations: bcc is preferred only at high charges and at low densities while fcc is dominant at higher densities. The solid phases melt upon the addition of salt: bcc may or may not transform to fcc before melting, depending on the particle number densities. No reentrant transition is found upon the addition of salt. When the particles are extremely highly charged, the system may undergo fcc–bcc–fcc transitions at nonzero salt concentration when the particle number density is increased.

I. INTRODUCTION

The study of the colloidal suspensions of electrically charged particles such as polystyrene or silica spheres has received much attention.[1] These colloidal systems can be regarded as scaled-up atomic systems with charges, particle sizes, and length scales 10^2–10^5 times larger than the typical atomic species. The particles constitute "ions" and, in the case of aqueous systems, the interaction between them is classically screened by either H_3O^+ or OH^-. The monodisperse suspensions are observed to be disordered (the "liquid" phase) at low densities and crystalline when the density is high.[1–9] The average interparticle distance is often in the order of the visible light wave length; and, hence the crystalline phase can Bragg-diffract visible light and thus result in opalescence. Most often, the crystalline structure is found to be face-centered-cubic (fcc).[2–4] In some dilute polystyrene suspensions where particles have high surface charges (in the order of 1000 electronic charges), body-centered-cubic (bcc) structure is found.[4–9]

Unlike their atomic counterparts, the interparticle interactions in colloids can be varied in a wide range by adjusting the parameters such as the salt concentration, the particle number densities, and the particle surface charge. It is therefore possible to talk about the phase diagram in the parameter space. So far, the calculated phase diagrams have either been based on an effective hard-sphere model[1] which is unable to produce a bcc phase, or based on solid-phase calculations[10] which did not treat the liquid phase adequately. Shih and Stroud[11] have done a two-phase calculation for the freezing but they did not look into the stabilities of various solid phases.

It is the purpose of this paper to calculate a more complete phase diagram by treating all the phases at equal footing. That is, the phase diagram will be calculated by directly comparing the Helmholtz free energy of different phases (bcc, fcc, hcp, and liquid) at the same parameters. In principle, one should draw a common tangent between the Helmholtz free energies of two different phases in the free energy vs particle number density in order to determine the phase-coexistence regions in the phase diagram; but, the theory is not accurate enough to allow this procedure. Our aim is then to get a correct qualitative account for the phase diagrams through our consistent way of treating different phases: the free energies of *all* phases are *calculated* via a variational principle based on the Gibbs–Bogolyubov inequality. Einstein oscillators are used as the reference systems for the crystalline phases and a hard-sphere fluid as that for the liquid. This procedure has been proven to give very good results for the polyvalent metallic systems.[12] We expect it to work well for the present case. The interparticle interaction is approximated to be the Debye–Hückel-screened Coulomb potential with size correction. The Debye–Hückel approximation is correct when the particle number density is low or the screening is weak, i.e., $qa_s \lesssim 1$, where q is the inverse screening length and a_s the average interparticle distance. Since our interest is to determine the phase boundaries in the part of the phase diagram where bcc is likely to appear, the Debye–Hückel-screened potential should then well represent the interparticle interactions in those regions where the particle number density is usually low.

We now turn to the body of the paper. Section II briefly describes the formalism. Section III gives the results and discussion. Some concluding remarks are given in Sec. IV.

II. FORMALISM

We consider an aqueous colloidal suspension of N spherical particles, each of radius a, in volume Ω, and at absolute temperature T. Each particle has an effective charge Z. The aqueous medium has a static dielectric constant. The NZ H_3O^+ or OH^- ions in the solution will neutralize the particles if no electrolyte is added to the solution. When the suspension is not too dense or the temperature is not too low, the interaction between particles can be adequately treated within the Debye–Hückel approximation. In MKSA units, the interaction takes the form

$$V(r) = \frac{Z^2 e^2}{4\pi\epsilon_0\epsilon}\frac{e^{-qr}}{r}, \tag{2.1}$$

where ϵ_0 is the permittivity of free space, ϵ is the static dielectric constant of the aqueous medium, e is the electronic

 0021-9606/87/095127-06$02.10 © 1987 American Institute of Physics

Downloaded 03 Feb 2006 to 128.112.35.206. Redistribution subject to AIP license or copyright, see http://jcp.aip.org/jcp/copyright.jsp

charge, r is the distance between particles, and q is the inverse screening length which satisifes

$$q^2 = \frac{e^2}{\epsilon_0 \epsilon k_B T} \sum_i n_i Z_i^2 , \tag{2.2}$$

where k_B is the Boltzmann constant, Z_i and n_i are the charge and the number density of the ith species of ions, respectively. In Eq. (2.1), the particles are assumed to be point-like. If the particles have a finite size, the interaction is modified as

$$V(r) = \frac{Z^2 e^2}{4\pi\epsilon_0 \epsilon} \left(\frac{e^{qa}}{1+qa} \right)^2 \frac{e^{-qr}}{r} , \tag{2.3}$$

where a is the radius of the particles. The factor $[e^{qa}/(1+qa)]^2$ takes into account the fact that the particles are not point-like and part of the volume in the solution is not available for screening because it is occupied by the particles. The size correction is important as is pointed out by Shih and Stroud[11] in order to avoid reentrant melting at high densities which is purely an artifact of the point-like interaction assumed in Eq. (2.1).

When the colloidal suspension is at equilibrium, its thermodynamic properties are determined by the Helmholtz free energy $F = E - TS$, where E is the internal energy and S the entropy. For a system of particles interacting via the potential (2.3), the free energy per particle F takes the following form:

$$F = \frac{1}{2N} \left(\frac{e^{qa}}{1+qa} \right)^2 \sum_{i \neq j} \frac{Z^2 e^2}{4\pi\epsilon_0 \epsilon} \left\langle \frac{1}{|\mathbf{r}_i - \mathbf{r}_j|} e^{-q|\mathbf{r}_i - \mathbf{r}_j|} \right\rangle + E_{\text{kin}} - TS , \tag{2.4}$$

where E_{kin} and S are the kinetic energy and the entropy per particle, $\langle\ \rangle$ denotes the thermal average over the canonical ensemble, and $\mathbf{r}_i$ is the position of particle i. Equation (2.4) includes only the terms of the free energy which depend on the arrangement of particles. These are the terms relevant in determining which structure (fcc, bcc, hcp, or liquid) is thermodynamically stable.

The free energy can be obtained from Eq. (2.4) by the use of a variational principle based on the Gibbs–Bogolyubov inequality[13] which states as follows:

$$F \leqslant F_0 + \langle U - U_0 \rangle_0 \equiv F' , \tag{2.5}$$

where F_0 is the free energy of the reference system and $\langle U - U_0 \rangle_0$ is the potential energy difference of the system of interest and the reference system, evaluated in the reference system. Since F is upper bounded by F', we can then approximate F to be the minimum of F' with respect to the appropriate variables, that is, $F \simeq F'(x_0)$ where

$$\left. \frac{\partial F'(x)}{\partial x} \right|_{x = x_0} = 0 , \tag{2.6}$$

where x is the appropriate variational variable.

We will use the Einstein oscillators for the solid as the reference system, and the Einstein frequency is chosen as the variational parameter, while a hard-sphere fluid will be the reference system for the liquid and the packing fraction will be the variational parameter. This procedure has been previously shown to give very good results for polyvalent metals[12]; and, thus we expect that it should work well in the present case.

A. Solid

The Einstein oscillators are used as the reference system: each particle oscillates independently about a lattice point in a harmonic potential well with a frequency ω. The Einstein frequency is to be used as the variational parameter. In the actual calculations for the colloidal systems, $\hbar\omega/k_B T$ is in the order of 10^{-7}–10^{-5}, much smaller than unity. Therefore, in terms of the Einstein temperature $\theta = \hbar\omega/k_B$, we may write

$$E_{\text{kin}} = \tfrac{3}{2} k_B T , \tag{2.7}$$

$$TS = 3k_B T [1 - \ln(\theta/T)] , \tag{2.8}$$

and

$$\left\langle \frac{1}{|\mathbf{r}_i - \mathbf{r}_j|} e^{-q|\mathbf{r}_i - \mathbf{r}_j|} \right\rangle = f(|\mathbf{r}_i - \mathbf{r}_j|) , \tag{2.9}$$

in which

$$f(r) = \frac{1}{2r} e^{wq^2} \left\{ e^{-qr} \left[1 - \text{erf}\left(\sqrt{w}q - \frac{r}{2\sqrt{w}} \right) \right] - e^{qr} \left[1 - \text{erf}\left(\sqrt{w}q + \frac{r}{2\sqrt{w}} \right) \right] \right\} , \tag{2.10}$$

where erf is the error function

$$\text{erf}(x) = \frac{2}{\sqrt{\pi}} \int_0^x e^{-y^2} dy , \tag{2.11}$$

and $3w$ is the mean square displacement which takes the following form:

$$w = \frac{\hbar^2 \coth(\theta/2T)}{2Mk_B\theta} , \tag{2.12}$$

in which M is the mass of the particles. Note that the anharmonic effect has been taken into account in Eq. (2.9). Combining Eq. (2.4) and Eq. (2.9), we get

$$F = \frac{1}{2} \left(\frac{e^{qa}}{1+qa} \right)^2 \sum_{\mathbf{R} \neq 0} \frac{Z^2 e^2}{4\pi\epsilon_0 \epsilon} f(|\mathbf{R}|) + E_{\text{kin}} - TS , \tag{2.13}$$

where $\mathbf{R}$'s are the lattice vectors. In the actual calculations, $r/(2\sqrt{w}) \pm \sqrt{w}q$ is much larger than unity and Eq. (2.10) reduces to

$$f(r) \simeq e^{wq^2} \frac{e^{-qr}}{r} . \tag{2.14}$$

B. Liquid

For the reference system, we use a fluid of particles interacting via the hard-sphere potential

$$U(r) = \infty , \quad r < \sigma , \text{ or} \qquad = 0 , \quad r \geqslant \sigma , \tag{2.15}$$

where σ, the hard-sphere diameter, is not, in general, equal to $2a$, the diameter of the actual particles. With this choice, the first term in Eq. (2.4) can be obtained analytically within the Percus–Yevick approximation, while the last term (the hard-sphere entropy) is available as an analytic fit to the

Downloaded 03 Feb 2006 to 128.112.35.206. Redistribution subject to AIP license or copyright, see http://jcp.aip.org/jcp/copyright.jsp

results of a Monte Carlo calculation. The liquid free energy thus takes the following form[14]:

$$F=\frac{Z^2e^2}{4\pi\epsilon_0\epsilon}\left(\frac{e^{qa}}{1+qa}\right)^2\frac{1}{r_0}[6\eta^{2/3}G(\lambda)] + \frac{3}{2}k_BT+\frac{k_BT\eta(4-3\eta)}{(1-\eta)^2}-TS_{ig}\,, \tag{2.16}$$

where $\frac{3}{2}k_BT$ is the kinetic energy per particle and r_0 is the Wigner–Seitz cell radius which satsifies

$$\frac{4\pi}{3}r_0^3=\frac{\Omega}{N}\,, \tag{2.17}$$

$\eta=(\pi/6)\sigma^3(N/\Omega)$ is the hard-sphere packing fraction, $\lambda\equiv 2\eta^{1/3}qr_0$, and

$$G(\lambda)=\lambda L(\lambda)/\{12\eta[L(\lambda)+\bar{S}(\lambda)e^{\lambda}]\}\,,$$
$$L(\lambda)=12\eta\left[\left(1+\frac{\eta}{2}\right)\lambda+(1+2\eta)\right]\,,$$
$$\bar{S}(\lambda)=(1-\eta)^2\lambda^3+6\eta(1-\eta)\lambda^2 + 18\eta^2\lambda-12\eta(1+2\eta)\,, \tag{2.18}$$
$$TS_{ig}=k_BT\ln\left[\frac{e\Omega}{N}\left(\frac{eMk_BT}{2\pi\hbar^2}\right)^{3/2}\right]\,, \tag{2.19}$$

where $e\equiv$natural number. The packing fraction η is the variational parameter for the liquid phase. It turns out that $\eta\simeq 0.45$ at freezing, which is consistent with Ref. 11 and also consistent with other polyvalent metallic systems.[12]

III. RESULTS

We have carried out calculations for the solid phases (fcc as well as bcc) and the liquid phase at various values of the particle number densities $D=N/\Omega$, charges Z, and the salt concentrations ρ with the procedure described in the previous section. The temperature T for all calculations is kept fixed at the room temperature since most of the experiment were done at that temperature. The static dielectric constant of water is taken to be 80. The phase diagrams are determined by comparing the free energies of different phases at the same parameter (the stable phase has the lowest free energy) and the phase boundaries are taken at the crossover points of the free energies of different phases.

A. Effect of Z and ρ

In order to directly compare with experiments, we first plot the results in the D–ρ plane at different values of Z. Figure 1 shows the D–ρ phase diagram of particles with $Z=400$ and different diameters. One can see that the colloidal suspension freezes when the particle number density is sufficiently high: The fcc phase is formed in most of the high-density region, whereas the bcc phase is stable only in a very narrow region of lower densities. The density range of the bcc phase shrinks as electrolytes are added to the solution, and the bcc phase completely disappears when the salt concentration is greater than about 2.5×10^{-8} M as seen in Fig. 1. Beside this, the addition of electrolytes will also make the crystalline phases become less favorable and eventually melt into liquid: The fcc phase always directly melts into liquid as

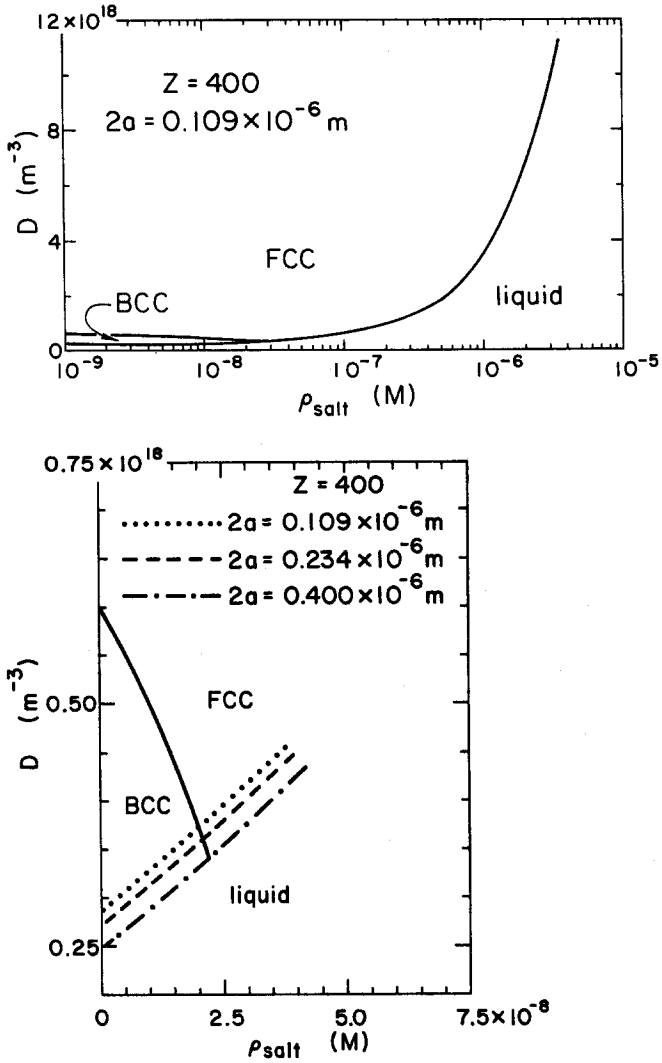

FIG. 1. D–ρ_{salt} phase diagram where D is the particle number density and ρ_{salt} is the added salt concentration in molar units; (a) for a particle diameter $2a=0.109\times10^{-6}$ m and charge $Z=400$; (b) in a different scale for $Z=400$ and diameters $2a=0.109\times10^{-6}$, 0.234×10^{-6}, and 0.400×10^{-6} m. The bcc–fcc phase boundaries are the same for the three cases while the liquid–solid phase boundaries are pushed to lower densities as the particle size is increased.

the salt concentration is increased, while the bcc phase can either transform into fcc before melting (at higher densities) or directly melts into the liquid phase (at lower densities). Note that there is no reentrant transition when the salt concentration is increased, and that the solid–liquid phase boundaries shift to higher densities when screening is increased by the addition of electrolytes.

In Fig. 2 we plot the D–ρ phase diagram for particles of the same size as Fig. 1(a) but with a smaller charge $Z=200$. Note that the bcc region is now absent and the solid–liquid phase boundary is pushed to a higher density. (Note the scale difference in Figs. 1 and 2.) Other than that, the solid–liquid phase boundary behaves roughly the same as that in Fig. 1, i.e., the solid phase becomes unstable when screening is increased. Again, this is in agreement with experiments. The shape of the solid–liquid phase boundary resembles very much that of the gold colloids in Ref. 15. These results sug-

Downloaded 03 Feb 2006 to 128.112.35.206. Redistribution subject to AIP license or copyright, see http://jcp.aip.org/jcp/copyright.jsp

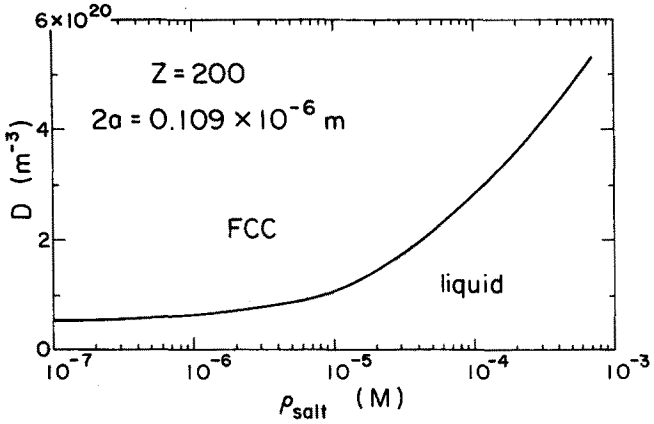

FIG. 2. D–ρ_{salt} phase diagram for particles with $Z = 200$ and $2a = 0.109 \times 10^{-6}$ m. Note that the bcc phase is missing when the particle charge is decreased. The definitions of D and ρ_{salt} are the same as in Fig. 1.

gest that the formation of a bcc crystalline phase in the colloidal suspension is a delicate matter: The bcc phase forms only when the electrolyte concentration is low and the particle charge is high, which is in agreement with experimental observations.[8,9] To better illustrate this trend, we plot in Fig. 3, the density range of the three phases as a function of the particle charge Z at zero salt concentration. The bcc region becomes narrower and finally closes up when Z is decreased. Meanwhile, Fig. 3 also shows that a large charge can retain the crystalline phases to a lower density.

Since a high surface charge of particles enables the crystalline phases to persist at low densities, with increasing particle charge, at some point, the solid phases may exist at such low densities that some finite amount of electrolytes could provide enough screening to favor fcc phase at low densities and therefore, an fcc–bcc–fcc re-entrant transition at some nonzero salt concentration is possible as the particle number

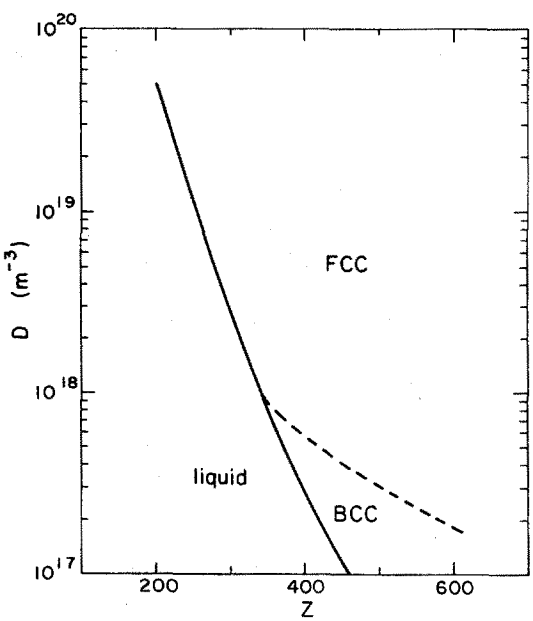

FIG. 3. The D–Z phase diagram for particles with diameter $2a = 0.109 \times 10^{-6}$ m and at zero salt concentration. bcc phase appears only when the charge Z is high and the particle number density D is low.

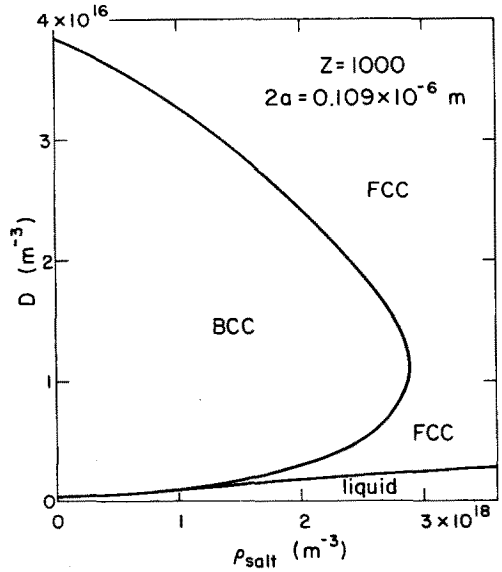

FIG. 4. The D–ρ_{salt} phase diagram for particles with diameter $2a = 0.109 \times 10^{-6}$ m and $Z = 1000$. Note that the system starts to undergo fcc–bcc–fcc transitions at fixed nonzero salt concentration when the particle number density is increased.

density is changed. Indeed, this can happen and is illustrated in Fig. 4 where particles of 0. 109 μm diam with $Z = 1000$ undergo an fcc–bcc–fcc transition as the density is varied at fixed salt concentration $\rho \gtrsim 1.3 \times 10^{18}$ m^{-3}. This can be explained as follows. At sufficiently low densities, the screening length does not vary much with the particle number density. (The major contribution to the inverse screening length comes from the added electrolyte concentration rather than the counter ions.) Under such conditions, the fcc phase is more stable at low densities because a given screening length would appear shorter when compared with the interparticle distance at low densities. We plot, as an example, in Fig. 5, the free energy difference between the fcc phase and the bcc phase as a function of the particle number density for particles of 1 μm diam and $Z = 4167$ when the inverse screening

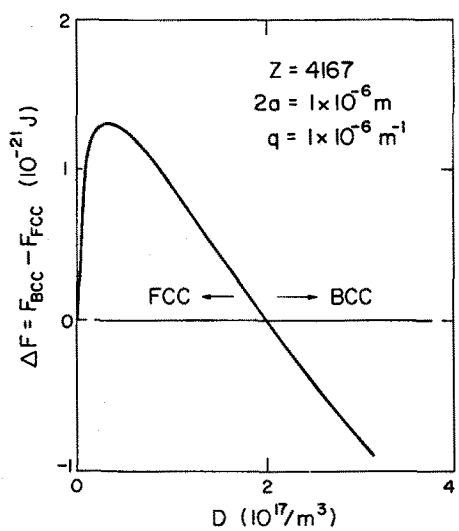

FIG. 5. Free energy difference between the fcc phase and the bcc phase as a function of the particle number density D.

Downloaded 03 Feb 2006 to 128.112.35.206. Redistribution subject to AIP license or copyright, see http://jcp.aip.org/jcp/copyright.jsp

length is fixed at $q = 1 \times 10^6\ \mathrm{m}^{-1}$. As the particle number density increases, the contribution of the counter ions to the screening becomes important again. We then recover the situation where the fcc dominates at high densities. So far, we did not include the screening by the electrolytes from the water itself. This is perfectly all right when the particle number density is not too low. However, when the particle density is low, the electrolytes of pure water can contribute substantially to the screening. Thus, the reentrant transition discussed above may be washed out by the intrinsic electrolytes of pure water and it is very likely that we may not be able to see it experimentally.

B. $\tilde{T}$–qa_s phase diagrams

If we define an effective temperature $\tilde{T} = k_B T/(Z^2 e^2/4\pi\epsilon_0\epsilon a_s)$ and measure the screening strength in terms of the dimensionless parameter qa_s where $a_s = (\Omega/N)^{1/3}$ is the average nearest neighbor distance, the phase boundaries in Figs. 1–5 should then be all mapped onto the same curves on the $\tilde{T} - qa_s$ plane. The phase boundaries in the $\tilde{T}$–qa_s plane are shown in Fig. 6. The liquid phase is stable at high $\tilde{T}$ and at large qa_s (i.e., small Z and high salt concentration). The bcc phase is preferred at small qa_s and fcc at large qa_s. There is no reentrant transition in either the $\tilde{T}$ or the qa_s direction. The $\tilde{T}$-independent bcc–fcc phase boundary is a result of the Debye–Hückel screened interparticle potential and can be explained as follows. First, within the physical range of $\tilde{T}$, the internal energy difference between two crystalline phases will change sign at the same qa_s as it does at $T = 0$. This can be seen from Eq. (2.14). The thermal vibration of the particles only magnifies the interparticle potential by a factor $e^{\omega q^2}$ for all pairs and does not change the sign of the difference of the lattice sums of two crystalline phases which is the consequence of the Debye–Hückel screened potential. (The kinetic energy which is $\frac{3}{2}k_B T$ for all phases is unimportant here.) For the entropy part, the Einstein frequency ω can be thought of as the average vibrational frequency of all modes and ω^2 is proportional to the average of the second derivatives of the interparticle potential at all particle sites which is $q^2 E_0$ within the Debye–Hückel approximation where E_0 is the $T = 0$ internal energy and q is the same for both phases at the same density. With the expression of TS in Eq. (2.8), one can readily see that the difference in $-TS$ between two crystalline phases has the same sign as that of the $T = 0$ internal energies and both change sign at the same qa_s. Therefore, the free energy difference between two crystalline phases always changes sign at the same qa_s as the $T = 0$ internal energy difference. The bcc–fcc phase boundary is thus independent of $\tilde{T}$.

C. Effect of particle size

We also plot phase boundaries of particles wth $Z = 400$ but of different diameters in Fig. 1(b). First, one can see that a larger particle size moves the solid–liquid phase boundary to a lower density. The discrimination of the liquid phase by the size correction factor is precisely what prevents reentrant melting at high densities. The bcc–fcc boundary is unaffected by the particle size. This size-independent bcc–fcc boundary is again the consequence of the Debye–Hückel screened potential. The size correction $(e^{qa}/1 + qa)^2$ is only a multiplying factor of the lattice sum, which does not change the sign of the internal energy difference of the bcc and fcc structures and hence does not change the sign of the free energy difference is argued above.

D. Is hcp structure possible?

Finally, we check the possibility of the hcp structure at high densities since the hcp phase has the same packing frac-

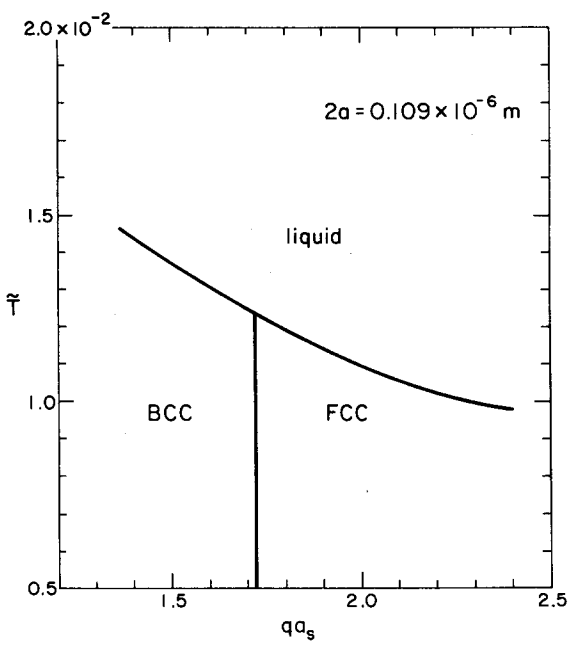

FIG. 6. The $\tilde{T}$–qa_s phase diagram for particles with diameter $2a = 0.109 \times 10^{-6}$ m. Where $\tilde{T}$, q, and a_s are as defined in the text.

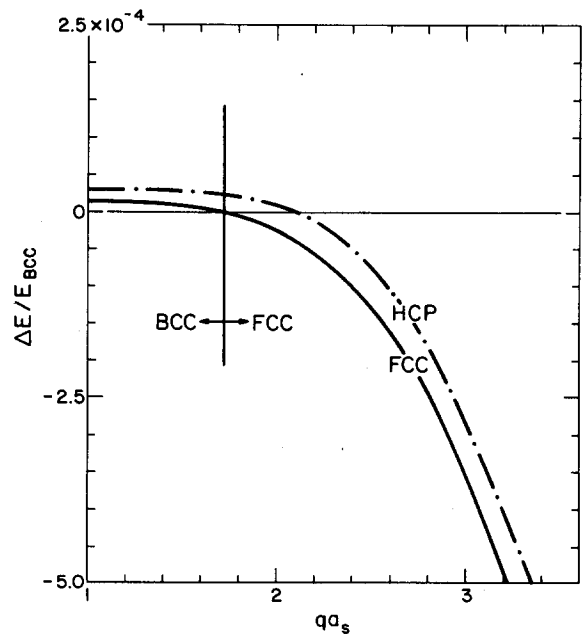

FIG. 7. The $T = 0$ energy difference $\Delta E/E_{\mathrm{bcc}}$ vs qa_s, where $\Delta E_{\mathrm{hcp(fcc)}} = E_{\mathrm{hcp(fcc)}} - E_{\mathrm{bcc}}$.

Downloaded 03 Feb 2006 to 128.112.35.206. Redistribution subject to AIP license or copyright, see http://jcp.aip.org/jcp/copyright.jsp

tion as the fcc phase at close packing. It turns out that the hcp phase is not favored throughout the entire qa_s range. Since the free energy difference changes sign at the same qa_s as the internal energy difference at $T=0$, we will show only the $T=0$ energy differences. In Fig. 7 we plot the $T=0$ internal energy difference of the hcp and bcc phases as well as of the fcc and bcc phases where $\Delta E_{\mathrm{hcp(fcc)}} = E_{\mathrm{hcp(fcc)}} - E_{\mathrm{bcc}}$. One can see that at small qa_s, the bcc phase is the stable state. At large qa_s, the internal energy of the hcp is lower than that of the bcc but is still higher than that of fcc. Although, the overall packing fraction is the same for both the fcc and hcp, the difference in the arrangement of far neighbors results in the difference in energy. So far, experimentally, hcp structures have only been observed when the system is under a shear stress,[5] which is obviously not an equilibrium state, in agreement with our results.

IV. CONCLUSIONS

We have determined the phase diagrams in the parameter space by directly comparing the Helmholtz free energies of different phases at the same parameters. The calculation of the free energies involves the use of a variational principle based on the Gibbs–Bogolyubov inequality and a Debye–Hückel-screened interparticle potential with size correction. We have shown that the colloidal suspensions can freeze into crystalline phases at higher densities. The fcc and bcc phases are the thermodynamically stable structures. The fcc phase is the dominant phase at higher densities while the bcc phase can exist at lower densities only when the particle charge is high and the salt concentration is low. Both crystalline phases will melt into liquid upon the addition of salt: fcc always melts into liquid directly, whereas bcc may transform into fcc before melting depending upon the particle number densities. No reentrant transition is found upon the addition of salt. However, highly charged particles can undergo an fcc–bcc–fcc reentrant transition at fixed nonzero salt concentrations when the particle number density is varied.

Our calculations have completely neglected the van der Waals attractions. This negligence is justified in the present case where the charges of the particles are in the order of 10^3 electronic charges and the densities are intermediate so that solid–liquid and bcc–fcc transitions can take place. Under such conditions, the interparticle interaction is dominated by the electrostatic potential. If the van der Waals attraction is taken into account, the phase boundaries should move to higher densities. Other than that, the phase diagram should remain qualitatively the same.

ACKNOWLEDGMENTS

The authors would like to thank W.-H. Shih for valuable discussions. This work was sponsored by the Defense Advanced Research Projects Agency of the Department of Defense and was monitored by the Air Force Office of Scientific Research under Grant No. AFOSR-83-0375.

[1]For a review, see P. Pieranski, Contemp. Phys. **14**, 25 (1983).
[2]W. Luck, M. Klier, and H. Wesslau, Ber. Bunseng. Phys. Chem. **57**, 75 (1963).
[3]P. A. Hiltner and I. M. Krieger, J. Phys. Chem. **73**, 2386 (1969).
[4]R. Williams and R. S. Crandall, Phys. Lett. A **48**, 225 (1974).
[5]B. J. Ackerson and N. A. Clark, Phys. Rev. Lett. **46**, 123 (1981).
[6]N. A. Clark, A. J. Hurd, and B. J. Ackerson, Nature **281**, 59 (1979).
[7]H. M. Lindsay and P. M. Chaikin, J. Chem. Phys. **76**, 3774 (1982).
[8]T. Yoshiyama, I. Sogami, and N. Ise, Phys. Rev. Lett. **53**, 2153 (1984).
[9]D. J. W. Aastuer, N. A. Clark, L. K. Cotter, and B. J. Ackerson, Phys. Rev. Lett. **57**, 1733 (1986).
[10]P. M. Chaikin, P. Pincus, and S. Alexander, J. Colloidal Interface Sci. **89**, 555 (1982); D. Hone, S. Alexander, P. M. Chaikin, and P. Pincus, J. Chem. Phys. **79**, 1474 (1983).
[11]W.-H. Shih and D. Stroud, J. Chem. Phys. **79**, 6254 (1983).
[12]Wan Y. Shih and D. Stroud, Phys. Rev. B **32**, 7779, 7785 (1985).
[13]See, for example, R. P. Feynman, *Statistical Mechanics* (Benjamin, New York, 1972); A. Isihara, J. Phys. A **1**, 539 (1968); D. J. Edwards and J. Jarzynski, J. Phys. C **5**, 1745 (1972).
[14]B. Firey and N. W. Ashcroft, Phys. Rev. A **15**, 2072 (1977).
[15]K. Takano and S. Hachisu, J. Colloid Interface Sci. **66**, 130 (1978).

Downloaded 03 Feb 2006 to 128.112.35.206. Redistribution subject to AIP license or copyright, see http://jcp.aip.org/jcp/copyright.jsp